ELSEVIER

Journal of Nuclear Materials 290–293 (2001) 820–824

journal of nuclear materials

www.elsevier.nl/locate/jnucmat

Experimental investigations of the SOL plasma in the MAST tokamak

J.-W. Ahn [a,b,*], G.F. Counsell [b]

[a] *Department of Physics, Imperial College, University of London, Prince Consort Road, London SW7 2BZ, UK*
[b] *Euratom/UKAEA Fusion Association, Culham Science Centre, Abingdon, Oxfordshire OX14 3DB, UK*

Abstract

Initial target plasma parameters have been obtained using Langmuir probe arrays in MAST DND plasmas. A clear in–out asymmetry was observed in the target parameters. All plasma parameter scale lengths were significantly elongated on the outboard side due to strong poloidal flux expansion. The electron temperature scale length λ_{Te} is typically 5–8 times broader than the density scale length λ_{ne}, suggesting a significant difference between heat and particle diffusivities in the SOL. A rough estimation of the SOL collisionality indicates that the inner SOL may be collisional ($v^* \sim 50$) whereas the outer SOL is marginally collisional ($v^* \sim 7$). The peak power density is about 4–5 times higher ($\sim$1 MW m^{-2}) on the inboard side, which has a SOL power density scale length $\sim$10 times narrower ($\sim$0.5 cm) than the outboard. The total power flow was approximately up–down symmetric, whilst the in–out power asymmetry was observed to be $P_{in} : P_{out} \sim 1 : 6.5$, exceeding the ratio of $\sim$1:3 for the inboard and outboard separatrix surface areas. A total of about 2/3 of the power entering the SOL reached the strike points (300 kW out of $P_{SOL} \sim 450$ kW).

Keywords: Power density; Divertor; SOL; Langmuir probe; MAST

1. Introduction

Divertor power loading is of critical importance to next-step tokamak fusion devices, where high heat and particle fluxes will determine the erosion and lifetime of divertor components and subsequent generation of impurities. These effects may be even more important in spherical tokamaks (STs) because of their smaller wetted areas, particularly on the inboard side. Characterisation of the scrape-off-layer (SOL) and strike point region in existing STs is thus crucially needed to provide basic data for SOL modelling, allowing extrapolation to larger devices.

The SOL plasma parameters and power loadings in double-null (DND) ST geometry were measured and analysed for the first time on START [1], where several unusual features were observed, including strong in–out/up–down power asymmetries, large flux expansions on the outboard side and significant SOL currents. However, analysis of the data was complicated by a blanket of high neutral density surrounding the START plasma (a result of the fuelling scheme, fully open divertor geometry and large vessel to plasma volume ratio), which was believed to give rise to large charge exchange losses from the SOL.

The larger successor to START, the mega ampere spherical tokamak (MAST) at Culham, has now been successfully commissioned and obtained first tokamak plasma in December 1999. The plasma performance at this initial stage includes up to 1 MA of plasma current, significant NBI auxiliary heating and clear access to H-mode (the main operating parameters are summarised in Table 1). Initial investigations of plasma conditions (including power loading) at each of the four strike points in MAST have been undertaken for a number of DND plasmas, with flat top plasma currents of about

* Corresponding author. Tel.: +44-1235 464 220; fax: +44-1235 464 192.
E-mail address: joon-wook.ahn@ukaea.org.uk (J.-W. Ahn).

0022-3115/01/$ - see front matter
PII: S0022-3115(00)00466-9

Table 1
Main operating parameters of MAST. Parameters for shot 2321 at time 144 ms are given on the right hand column as well as the general parameter ranges on left

Operating parameters	Design range	Shot 2321
Major radius R (m)	0.7–0.85	0.82
Minor radius a (m)	0.5–0.65	0.57
Plasma current I_p (MA)	$\leqslant 2$	0.44
Aspect ratio A	$\geqslant 1.3$	1.44
B-field on axis, B_0 (T)	$\leqslant 0.6$	0.4
P_{AUX} (MW)	$\leqslant 6.5$	0
Pulse length (s)	$\leqslant 5$	0.15
$n_e(\times 10^{19}\ m^{-3})$	1–10	~ 1

500 kA and average electron density of around 10^{19} m^{-3}. The results are presented together with initial data indicating that, as expected from modelling [2], neutral densities in the MAST vessel are substantially lower than in START, removing the uncertainties introduced by large charge exchange losses.

2. Experimental setup

MAST is well equipped with arrays of high spatial resolution, swept Langmuir probe arrays (576 probes in total) covering all four strike point regions. The inboard strike points (ISPs) fall on the ~20 cm diameter centre column. This is protected by graphite tiles in which there are 212 flush-mounted probes spaced 3 mm apart and arranged in two arrays covering the upper and lower ISP regions. The outboard strike points (OSPs) fall on a series of radial divertor ribs, two of which (one upper and one lower) are installed with arrays of 90 flush-mounted probes, spaced 10 mm apart.

Groups of up to 16 probes are served by a multiplexer unit distributing the applied voltage sweep from a single amplifier. Each individual voltage sweep typically has a period of ~200 μs, resulting in an average time resolution for each multiplexer channel of ~3 ms. A total of 192 probes are operated simultaneously by 12 amplifiers. A novel technique [3], which optimises the voltage sweep by offsetting to the local floating potential (V_f), has been used to drive these probes. Prior to each sweep, the local V_f is measured with a high input impedance voltage follower, and held on a 'sample-and-hold' unit. During the sweep, the sampled voltage is added to an externally applied sweep waveform ensuring that it is optimally located to obtain both ion saturation and electron retardation regions of the characteristic.

A typical MAST pulse length is currently ~300 ms, which is nearly six times longer than that in START. However, only data taken from after the formation of a clear DND configuration (Figs. 1 and 2), with the inboard separatrix well separated from the centre column, were analysed. Care was taken to select data for well-established plasmas, with low levels of MHD activity, and for which quality data was available at all four strike points simultaneously.

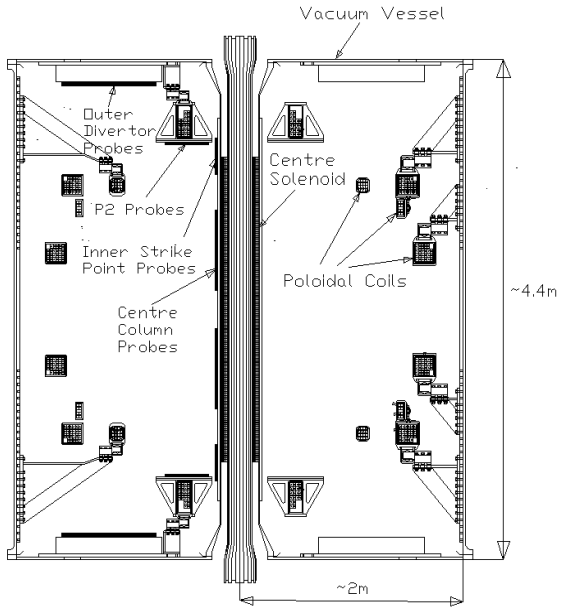

Fig. 1. A schematic view of MAST Langmuir probe arrays.

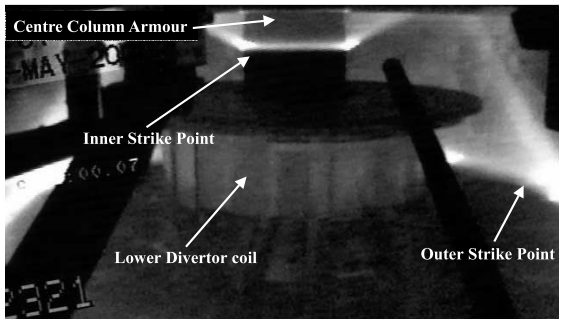

Fig. 2. Visible light image for shot 2321 (Ohmic only), showing lower inner and outer strike points at time 140 ms.

3. Analysis

Following conventional practice, T_e was derived by fitting exponentials to the I–V characteristics, only in the region from ion saturation to just beyond floating potential, in order to avoid distortion of the characteristic resulting from early saturation of electron current [4]. As on START, the geometric probe area was used for obtaining n_e and power density q, instead of its projection

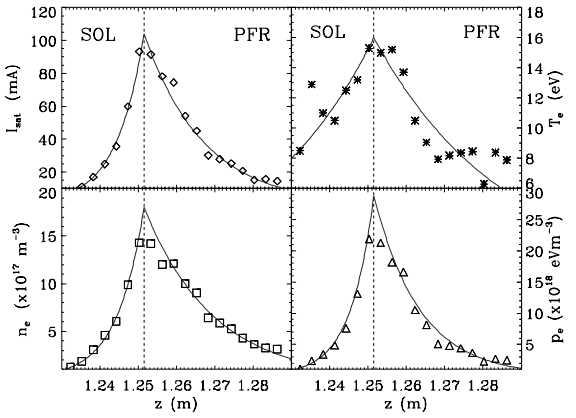

Fig. 3. Plasma parameter profiles across the upper ISP at time 144 ms for shot 2321. Peak I_{sat} is regarded as the separatrix location.

perpendicular to the local field, to allow for the effect of large ion Larmor radii experienced in the relatively low field of MAST ($\sim$0.3 T on the outboard side). The power density at each probe was calculated using $q = \delta J_{sat} T_e$, where the sheath power transmission factor (δ) was taken as 7 (assuming equal electron and ion temperatures and no secondary electron emission).

The temperature, density and power density scale length and separatrix values can be derived from exponential fits to the plasma parameter profiles (Fig. 3). The separatrix is usually identified from the peak in the ion saturation current. Total power flow to the inboard and outboard strike points were then determined by integrating over the total surface area of the strike point assuming an exponential profile for the power density.

$$P = \int_0^\infty 2\pi R q^{sep} e^{-x/\lambda_q^{SOL}} dx + \int_0^\infty 2\pi R q^{sep} e^{-x/\lambda_q^{PFR}} dx$$
$$= 2\pi R q^{sep} (\lambda_q^{SOL} + \lambda_q^{PFR}),$$

where P is the power in SOL and private flux region (PFR) in the strike point region, R the radius of separatrix at target, x the radial or vertical coordinate (vertical for inboard, radial for outboard), λ_q the power density scale length and q^{sep} is the power density at the separatrix.

4. Results

4.1. Target parameter results

Fig. 3 shows the profiles of ion saturation current (I_{sat}), electron temperature (T_e), electron density (n_e) and electron pressure (p_e) across the upper ISP. They are well established and show a clear exponential fall-off (except, perhaps, for T_e, the analysis of which is subject to the largest uncertainties). Similar sets of data were obtained for each of the other three strike points. The raw data for the ISP showed much lower levels of noise than the outboard one, where uncertainties in the electron temperature of at least a factor 1.5 or so were introduced (depending on exactly which portion of the I–V characteristic was analysed). Since the density and pressure inferred depend on the temperature used, the error bars for these are correspondingly large (perhaps $\pm$30–50% for the outboard data compared to perhaps $\pm$20% for the inboard).

The target profile data are summarised in Table 2, together with line integrated values of n_e and p_e across the profiles. The higher density and lower temperature on the inboard side is offset by a narrower strike point width giving similar line integrated values for the ISP and OSP. No clear evidence for up/down asymmetries in both the separatrix and integral values within the error bar is observed. However, by far the largest asymmetry is that between the inboard and outboard temperature and density scale lengths, which are $\sim$10 times larger on the outboard side as a result of strong poloidal flux expansion. This effect is also observed in measurements of the separatrix density, which is substantially lower on the outboard side.

One more interesting observation relates to the temperature and density decay lengths. At three of the four strike points, the ratio $\lambda_{Te} : \lambda_{ne}$ lies between 5 and 8, perhaps indicative of a significant difference between heat and particle diffusivities in the SOL (the ratio at the lower OSP is just 2.4 for reasons which remain to be understood).

Table 2
Summary of the target profile data for shot 2321 at time 144 ms. dl is the elemental length along the divertor tile, i.e., in the z direction for the inboard profiles and in the R direction for the outboard profiles

Parameter	Strike point location	
	Inboard	Outboard
Upper		
T_e^{sep} (eV)	16 ± 5	17 ± 8
n_e^{sep}($\times 10^{17}$ m^{-3})	18 ± 3	3.2 ± 1
λ_{Te}^{SOL}(cm)	3.1 ± 0.9	43 ± 21
λ_{ne}^{SOL}(cm)	0.71 ± 0.1	5.7 ± 1.7
$\int n_e dl$($\times 10^{16}$ m^{-2})	4.2 ± 0.7	3.6 ± 1.1
$\int p_e dl$($\times 10^{17}$ m^{-2} eV)	4.8 ± 2.2	5.1 ± 3.5
Lower		
T_e^{sep} (eV)	16 ± 8	20 ± 10
n_e^{sep}($\times 10^{17}$ m^{-3})	13 ± 4	2.0 ± 0.6
λ_{Te}^{SOL}(cm)	4.4 ± 2.2	27 ± 14
λ_{ne}^{SOL}(cm)	0.76 ± 0.23	11 ± 3.4
$\int n_e dl$($\times 10^{16}$ m^{-2})	6.0 ± 1.8	5.1 ± 1.5
$\int p_e dl$($\times 10^{17}$ m^{-2} eV)	7.7 ± 5.4	8.6 ± 6.0

4.2. Power to the target plates

Estimates of power flow to the strike points are summarised in Table 3. The peak power flux densities show significant in/out asymmetry at both upper and lower targets, with the inboard tiles subject to 4–5 times higher density than the outboard ones.

The total power flow to each target was estimated by integrating across the power density profile. For the inboard side, an extended trapezoidal method [5] was used to estimate the area under the profile, which was then multiplied by $2\pi R$ (where R is the major radius of the centre column armour) to account for the toroidal extent. On the outboard side, because the major radius varied across the profile, a variant on the trapezoidal method was used to estimate the power received by each target. In this method, the profile is divided into N annuli of area $\pi(R_{i+1}^2 R_i^2)$, where R_i is the major radius of the ith chord. The power contained within each annulus is then $(q_{i+1} + q_i)/2$, where q_i is the power density at the i chord. The sum of power contained within each annulus then gives the power to the target:

$$P = \sum_i (R_{i+1}^2 - R_i^2) \frac{q_{i+1} + q_i}{2}.$$

The power flowing into the outboard side is typically 5–8 times higher than that into the inboard side while the total power flowing to each of the upper and lower divertor targets is approximately the same (~150 kW), giving a grand total of ~300 kW.

Fig. 4 shows the power density profiles on the outboard side at both upper and lower targets with fitted exponential fall-off curves. No marked difference between upper and lower profiles was observed (apart from a shift in the radial position, resulting from a vertical displacement of the core plasma). The SOL heat flux width at the inner strike point is typically around 0.5 cm (and longer than 1.0 cm in the PFR), whilst that at the outer strike points exceeds 5 cm (and 4–6 cm in the PFR). This gives a value of ~1.5 cm for the inner total strike point width and ~10 cm for the outer width (a result of strong outboard flux expansion in the ST).

Table 3
Summary of the power flow result for shot 2321 at time 144 ms

Parameter	Strike point location	
	Inboard	Outboard
Upper		
q^{sep}(MW m^{-2})	1.05 ± 0.2	0.20 ± 0.6
λ_q^{SOL}(cm)	0.53 ± 0.1	4.8 ± 1.4
Power (kW)	21 ± 4	137 ± 41
Lower		
q^{sep}(MW m^{-2})	1.05 ± 0.3	0.18 ± 0.05
λ_q^{SOL}(cm)	0.61 ± 0.2	6.6 ± 2
Power (kW)	23 ± 7	118 ± 35

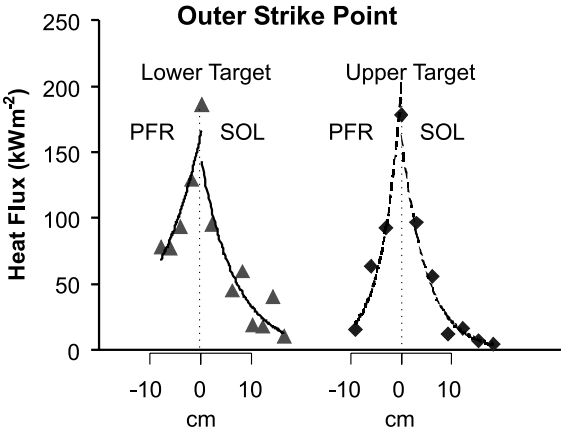

Fig. 4. Heat flux density profiles on the outboard side for shot 2321 at time 144 ms.

4.3. Estimate of the SOL collisionality

Rather more speculative, given the preliminary nature of the data, is an estimate of the SOL collisionality which is often characterised in terms of the quantity $\nu^* = L/\lambda_{ee}$, where L is the parallel connection length and the electron–electron mean free path, λ_{ee}, which may be defined as:

$$\lambda_{ee} = v_{Th}\tau_{ee} = \sqrt{\left(\frac{3kT_e}{m_e}\right)}\tau_{ee},$$

and

$$\tau_{ee} = \frac{\sqrt{3}6\pi\varepsilon_0^2}{e^4} \frac{\sqrt{m_e}(kT_e)^{3/2}}{n_e \ln\Lambda} \approx 2.4 \times 10^{11} \frac{T_e^{3/2}[\mathrm{eV}]}{n_e[\mathrm{m}^{-3}]\ln\Lambda}.$$

However, implementation of magnetic reconstruction code on MAST is still incomplete and L is not generally available. As a result, only rough estimation of the collisionality is possible. Typical, measured values of target density (~3×10^{17} m^{-3}) and temperature (~15–25 eV) at the OSP, combined with L of around 50 m (scaled up from the START data), indicate that the outboard SOL is marginally collisional ($\nu^* \sim 7$). However, a higher density (~1.5×10^{18} m^{-3}) and slightly lower temperature (10–20 eV) at the inner strike points, together with L of around 40 m, suggests that the inner SOL may be collisional in nature ($\nu^* \sim 50$). Here, the non-intuitive, similar parallel connection lengths on the inboard and outboard side result from a balance between the major radius ($R_{in} \ll R_{out}$) and toroidal field ($B_\phi^{in} \gg B_\phi^{out}$), and hence field line pitch, at tight aspect ratio.

5. Discussion

The power flowing into the SOL can be estimated as

$$P_{\mathrm{SOL}} \approx P_{\mathrm{VI}} - \frac{d}{\mathrm{d}t} W_{\mathrm{MAG}} + P_{\mathrm{BEAM}}^{\mathrm{abs}} - \frac{d}{\mathrm{d}t} W_{\mathrm{KIN}} - P_{\mathrm{RAD}},$$

where W_{MAG} is the energy stored in the magnetic field, $P_{\mathrm{VI}} - dW_{\mathrm{MAG}}/\mathrm{d}t$ the net ohmic heating power, W_{KIN} the kinetic energy of the plasma, P_{BEAM} the absorbed beam power (0 for shot 2321, Ohmic only) and P_{RAD} the radiated power from the confined region. It is difficult to make an accurate estimate at this stage of the Ohmic power input to the plasma, as the plasma was evolving at this time and reliable estimates of $\mathrm{d}W_{\mathrm{MAG}}/\mathrm{d}t$ are not yet available. However, making the assumption that the plasma was stationary and that about 40% of power was lost by radiation, we can estimate the net SOL input power as $P_{\mathrm{SOL}} \approx 0.6 P_{\mathrm{VI}} \sim 450$ kW for shot 2321. This means that about 2/3 of the power entering the SOL arrives at the divertor tiles. This value is contrasted by START results, which had typically only about 1/3 of P_{SOL} arriving at the divertor tiles [1]. This difference may be explained by a reduced level of charge exchange collisions in the MAST SOL compared to START, a result of much lower neutral density (~50 times) in the MAST vessel (of about $1–10 \times 10^{17}$ m^{-3}), which had been anticipated by modelling [2].

A useful ratio is that of the outboard to inboard total power efflux. At ~6.5, this ratio is significantly in excess of the geometric ratio of outer to inner separatrix surface area which, for a typical DND equilibrium, is around 3. This is similar to observations from START [3] and indicates that geometric effects in the ST are being augmented by increased transport on the outboard side, possibly resulting from steep gradients in the flux surface parameters (arising from the large Shafranov shift in the ST) coupled with enhanced MHD losses at the outboard side (resulting from the lower field and unfavourable curvature).

Interpretative modelling of the MAST SOL plasma using the onion–skin method (OSM) [6] is about to be undertaken and should give significant insight into relationships between the edge plasma parameters and allow extraction of information about cross-field transport coefficients, which may be significantly different in the ST SOL (which exhibits strong divertor throat mirrors and large ion Larmour radii).

6. Conclusions

Measurements of target parameters in MAST DND plasmas have been made using arrays of Langmuir probes across the strike point regions. The divertor plasma was rather cool (~20 eV) and had a relatively low density ($0.25–1.5 \times 10^{18}$ m^{-3}). A clear in/out asymmetry in plasma parameters was observed in the target profiles on both the upper and lower plates. All the plasma parameter scale lengths were elongated on the outboard side as a result of strong flux expansion. The peak power density at the ISP is about 4–5 times higher (~1 MW m^{-2}) than the OSP for the Ohmic plasmas considered, but with a strike point width nearly 10 times as narrow (~1.5 cm).

The total power incident on the targets has also been calculated from the probe data. This power seemed to be approximately evenly distributed between the upper and lower targets in each SOL, within experimental uncertainty, but a strong in–out asymmetry was observed. The ratio of the average power to the inboard targets to the average power to the outboard targets was ~1:6.5. This exceeds the ratio of ~1:3 for the inboard and outboard separatrix surface areas. About two-thirds of the power entering the SOL reached the target compared to one-third on START (the difference probably arising from higher charge exchange losses in the latter). A rough estimation of the SOL collisionality suggests that the outer SOL may be marginally collisional ($\nu^* \sim 7$) and the inner SOL collisional ($\nu^* \sim 50$).

Work is on-going to implement OSM analysis techniques for the MAST SOL and supplement target probe data with upstream measurements from reciprocating probe and helium line ratio diagnostics.

Acknowledgements

The authors would like to thank Mike Smith for help in commissioning electronics for the probe data acquisition. Marcus Price and Ken Axon also deserve an appreciation for generating the photographic images. This work was jointly funded by the UK Department of Trade and Industry and Euratom. One of the authors (J.-W.A.) would like to acknowledge both the British Council and UKAEA Fusion for financial support.

References

[1] K.M. Morel, J. Nucl. Mater. 266–269 (1999) 1040.
[2] G.P. Maddison, in: Proceedings of the 26th EPS Conference on Control Fusion and Plasma Physics ECA, vol. 23J, 1999, p. 241.
[3] K.M. Morel, PhD thesis, University of London, October 1999.
[4] J.A. Tagle et al., Plasma Phys. Control Fus. 29 (1986) 297.
[5] Numerical Recipes: The Art of Scientific Computing (FORTRAN). Cambridge University, Cambridge, 1990.
[6] K. Shimizu et al., J. Nucl. Mater. 196–198 (1992) 476.